Available online at www.sciencedirect.com

ScienceDirect

Scripta Materialia xxx (2015) xxx–xxx

Scripta MATERIALIA

www.elsevier.com/locate/scriptamat

Three-dimensional effects of twinning in magnesium alloys

K. Hazeli,[a] J. Cuadra,[b] F. Streller,[d] C.M. Barr,[c] M.L. Taheri,[c] R.W. Carpick[d] and A. Kontsos[a,*]

[a]*Department of Mechanical Engineering & Mechanics, Drexel University, USA*
[b]*Department of Materials Science & Engineering, University of Pennsylvania, USA*
[c]*Department of Materials Science & Engineering, Drexel University, USA*
[d]*Department of Mechanical Engineering & Applied Mechanics, University of Pennsylvania, USA*

Received 18 October 2014; revised 29 November 2014; accepted 1 December 2014

This article provides experimental evidence on the pronounced three-dimensional surface effects caused by tension twinning at early stages of plasticity of a magnesium alloy. To achieve this goal, multiscale mechanical testing was combined with strain field, texture and surface morphology quantification. The current investigation correlates crystallography-driven, grain-scale surface roughening to the spatially heterogeneous micro- and macrostrain. It was found that tension twinning causes considerable surface extrusions and intrusions across multiple grains that are directly related to severe strain inhomogeneities.

Keywords: Twinning; Surface step; Strain localization; Digital image correlation (DIC); Local plasticity

Understanding twinning, including nucleation of different variants, their growth and interactions with other deformation modes, is a topic of increasing interest for hexagonal close-packed (hcp) alloys due to its role in plasticity [1]. Because of its relatively easy activation, much attention has been paid to $\{10\bar{1}2\}$ tension twinning [2–5]. Thompson and Millard [6] and Yang et al. [7] performed experimental analyses on cadmium and titanium respectively, based on which they suggested that lenticular twins resulted in step formations between two $\{10\bar{1}2\}$ lattice planes at the twin boundary. Furthermore, recent studies based on molecular dynamics simulations and electron backscattered diffraction (EBSD) data provided further evidence on twin nucleation [1,8–10]. The statistical analysis of twin nucleation presented by Beyerlein et al. [1] indicated that grain boundary misorientations influence twin nucleation and growth. It has also been proposed that the stress states in the vicinity of grain boundaries dictate the prevalence of specific twin variants [11].

In addition to the considerable effect of twinning on ductility [12,13], a study by Kocks and Westlake [14] and another by Hutchinson [15] suggested that the ductility of polycrystalline hcp metals is affected by local strain variations in neighboring grains. While boundaries clearly cause heterogeneous strain in adjoining crystals, it is not clear how this strain affects the cohesive properties of the grain boundary, because a strongly cohesive boundary may force heterogeneous strain in an adjacent grain to maintain compatibility. The local high strain concentration may therefore cause microcracks [16]. It has also been suggested that twinning is associated with crack formation at later stages of deformation [17–19]. Therefore, besides some of the known sources of crack initiation, such as surface roughness, inclusions, intermetallic and ductile/brittle phases [20], twinning, slip and strain inhomogeneities at the grain scale can be also envisioned as other sources of crack incubation and initiation [21]. In agreement with Muránsky et al. [22] and Barnett et al. [23], the authors recently demonstrated [24] that the onset of the distinct plateau region in the stress–strain curve during compressive loading perpendicular to the *c*-axis is associated with profuse and spatially inhomogeneous twinning. We recently showed that, although tension twinning could further give rise to crack initiation towards the end of the fatigue life in Mg alloys [25].

Similar to the earlier study by Vaidya and Mahajan [26], in which evidence of slip on $\{11\bar{2}1\}$ planes prior to twinning was reported, Koike et al. [3] demonstrated that twinning occurs in grains with high basal dislocation activity. Therefore, as Hull [18] and more recently Ando et al. [17] suggested that localized strain inhomogeneities resulting from the activation of slip can presumably be relieved by twinning. It is also plausible that stress concentrations due to incompatibilities between twins and their surrounding matrix regions can be relaxed by slip [17,26] or crack formation [12].

In order to explain the relationship between grain-scale microstructural changes and deformation in alloys, a number of recent investigations relied on the use of the digital image correlation (DIC) method [27–33]. Carroll et al. [32] combined ex situ texture measurements with

* Corresponding author; e-mail: akontsos@coe.drexel.edu

http://dx.doi.org/10.1016/j.scriptamat.2014.12.001
1359-6462/

high-resolution strain field mapping obtained by DIC to explain strain localizations near grain boundaries. Furthermore, Dave et al. coupled incremental straining of nickel foils with optical microscopy and showed the effect of grain boundaries and orientation mismatches on localized strain distributions [30].

In this letter, full-field deformation measurements in Mg alloys were first performed at the grain scale. A cube-shaped specimen consisting of grains with most of their *c*-axis perpendicular to the loading direction was prepared from a commercial AZ31 plate. A region of interest (ROI) of 1 mm^2 size was defined by using fiducial markers created by micro-hardness indentations. The sample was loaded utilizing an MTI/Fullam (SEMaster 1000 EBSD) stage at a compressive displacement rate of 0.5 mm min^{-1} up to about 2% overall strain. An optical microscope (Olympus BH-2) was fixed at 10 × magnification to record image sequences during loading. The images were recorded by a 10 megapixel camera with a 25 Hz acquisition rate. The gray intensity (contrast) field captured by the camera was created by the alloy microstructure without any additional surface patterning. Two-dimensional deformation measurements were performed in a field of view of 900 × 675 μm^2, which resulted in a maximum spatial resolution for deformation measurements of 11.25 $\mu m\ pixel^{-1}$. The recorded digital images were post-processed using the commercially available ARAMIS GOM software (v6.30-4). A smaller ROI of 196 × 239 μm^2 at a specific location was analyzed to compute more accurate full-field and point strains. The surface morphology was inspected post-mortem by non-contact white light interferometry using a Zygo surface profilometer (model 6300) at 20× magnification. A lateral resolution of 750 nm and a vertical resolution of 0.1 nm were achieved. Note that, the orientation and topography for the deformed samples were performed without any further polishing or etching.

To validate the surface morphology observations at the grain scale, compression tests on cylindrical specimens of (ASTM) standard dimensions were also performed. The samples were flattened on one side to allow post-mortem microstructure analyses and then mechanically compressed with a strain rate of $4.5 \times 10^{-4}\ s^{-1}$. Prior testing, the specimens were subjected to the polishing procedure described previously [34]. Fiducial markers on the polished surface were produced by microhardness indentation. The surface morphology in the ROI (250 × 250 μm^2) was quantified using the interferometry method used for the grain-scale tests. Full-field strain fields were measured using DIC. The full-field strain measurement setup was capable of resolving strains with an accuracy of ± 150 $\mu m\ m^{-1}$ and a resolution of 20 $\mu m\ pixel^{-1}$.

Figure 1(a) shows twin nucleation and growth observed in situ by the optical microscope on the grain-scale specimen subjected to compression. Figure 1(b) displays the corresponding full-field strain evolution parallel to the loading direction, marked as global strain. Figure 1(c) plots the average global strain as a function of time. It also presents point-to-point measured strain values across the twin region highlighted in Figure 1a and b. This measurement shows how the local strain field within a grain develops as a result of twinning. The measured local and global strains demonstrate that, while the sample undergoes compression (see the black line in Fig. (1)c), favorable grains (G1 and G2) for twinning, according at least to the reported high Schmid factor (SF) criterion [35], display large tensile strains exactly at twin locations. It has been proposed by the authors [34] that strain localizations associated with twinning first initiate at grains with larger SF values [36,37].

Although the theoretical maximum tensile strain caused by twinning in Mg single crystal has been reported to be 6.5% [38], the current results provide locally considerably larger values which are suspected to be related to 3-D surface effects of twinning. It is known that out-of-plane motion directly affects any 2-D (in-plane) strain measurements. This was verified in Figure 1(e), which shows examples of pronounced surface morphology changes (differences in height are represented by a color bar in micrometers)

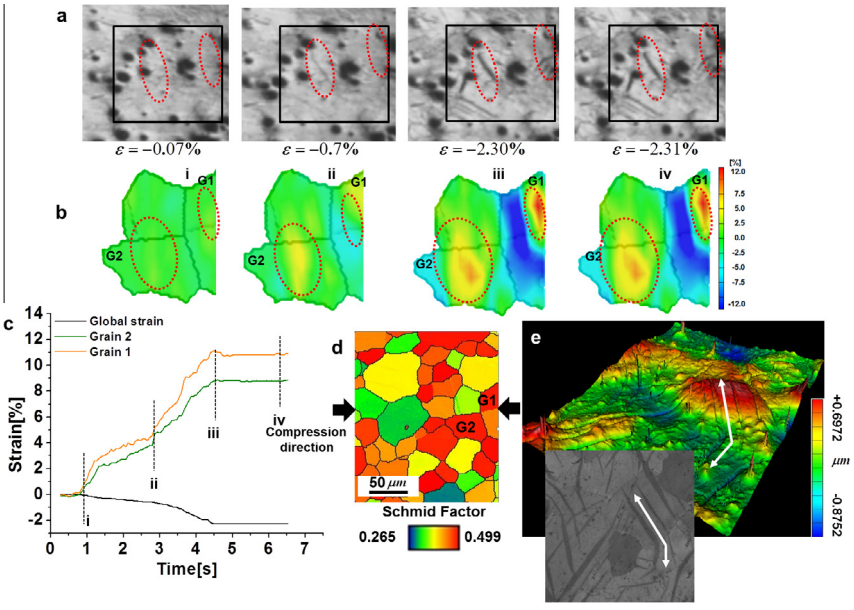

Figure 1. (a) Optical microscope images of twin nucleation and growth obtained in situ. (b) Full-field strain maps obtained by DIC with overlaid grain structure. (c) Local (for two different grains) and global (average) strain evolution in time. (d) Measured SF values in the ROI. (e) 3-D views of the surface contour displaying grain-scale extrusions and intrusions, and their close relationship to twinning.

Please cite this article in press as: K. Hazeli et al., Scripta Mater. (2015), http://dx.doi.org/10.1016/j.scriptamat.2014.12.001

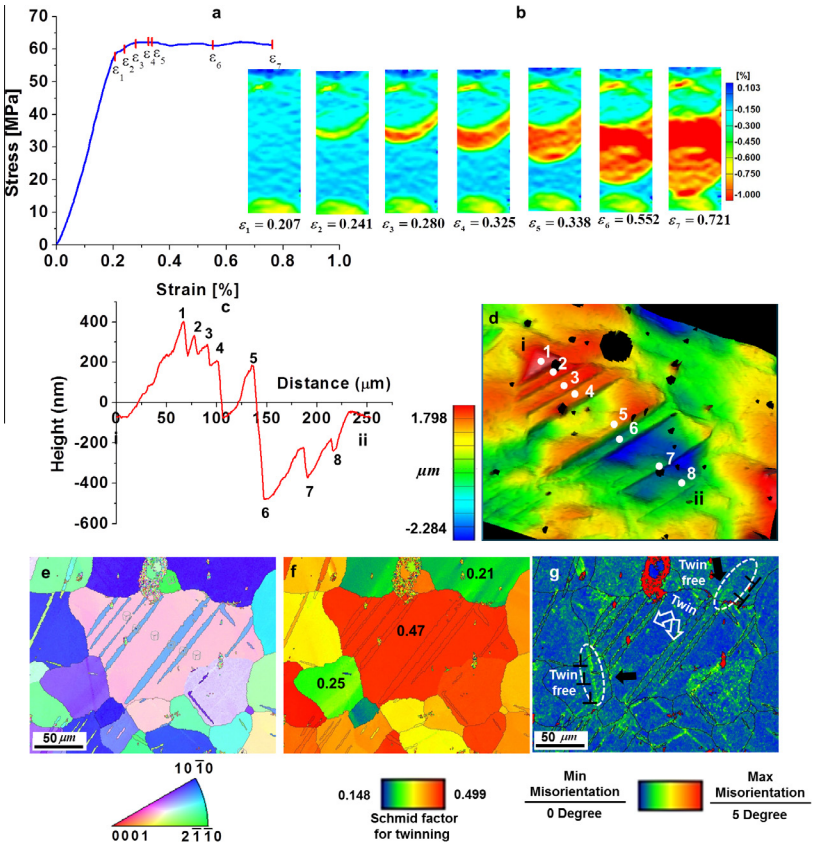

Figure 2. (a) Interrupted stress–strain curve (ε 1% of total strain) for a cylindrical compression sample. (b) Full-field longitudinal (parallel to the loading axis) strains for seven increments marked on the stress–stain curve. (c) Surface step profile from a line scan identified by points (i) and (ii) in the morphology map in (d) obtained from white-light interferometry. (e) IPF for the same set of grains. (f) Corresponding SF values and (g) KAM maps.

obtained using the interferometry method. Large extrusions and intrusions in grain regions dominated by twinning revealed a complex surface relief. The formation of such surface steps due to twinning were previously reported to occur in later stages of plasticity during compression of Mg alloy samples [17]. However, to the best of our knowledge, this is the first study that reports surface step formation as a result of twinning and its associated strain fields at early stages of plasticity in Mg alloys. Similar to the results reported in this letter, out-of-plane components of strain due to slip and twinning were observed during four-point bending experiments on a titanium alloy [7].

Figure 2(a) demonstrates the yielding and post-yielding mechanical behavior in the stress–strain curve obtained by compression of cylindrical specimens. To investigate the microscale plasticity the applied loading was interrupted while the strain was less than 1%. Figure 2(b) presents the average full-field strain evolution along the loading direction for the strain stages marked with numbers in Figure 2(a). The strain maps suggest that the onset of yielding is coincident with distinct strain localizations. The results in Figure 2c and d validate the findings reported in Figure 1 that relate early plastic deformation to pronounced surface steps at the grain scale. Thorough microstructural examination of regions from inside the strain band shown in Figure 2(b) revealed surface steps quantified by the height vs. distance curve (along the points numbered as (i) and (ii) in Figure (2)c), which provides the size of extrusions and intrusions on the surface of the one-side-flattened cylindrical specimen. Moreover, Figure 2e–g provide the texture, SF values and kernel average misorientation (KAM) map, respectively, for the same ROI. It can be seen in Figure 2f that the grain with an SF of 0.25 did not undergo twinning, unlike the one with an SF of 0.47, which contains several twins. This observation provides some evidence of the role of SF in twinning [1]. Additionally, Figure 2g shows distinct areas with pronounced local misorientation marked with white dashed ellipses near the grain that twinned. Such KAM maps have been related to the stored strain energy [35,39,40]. It is evident via the KAM that the density of dislocations at critical intersections of grain boundaries and twins (marked with solid black arrows in Figure 2g) is relatively higher. This observation may support model suggested by Meyer et al. [41] and the experimental study by Koike et al. [3], which suggest that stress concentrations are caused by the pronounced activation of basal slip prior to twinning. In agreement with a recent study by Balogh et al. [42]. For example, Figure 2(d) shows the occurrence of several twins in one grain, providing a strong indication that twin dislocations could also be driven by variable stresses [42].

The twin path in relation to local misorientation, SF values and surface step geometry is investigated in Figure 3. It is shown in this figure that twins tend to form in grains with high SF values (0.46–0.48), while thickening occurs in energetically favorable paths (longer side of the grain). Moreover, it is expected that, as local internal stresses increase due to dislocation pile ups and activation of non-basal slip, subgrain recrystallization nuclei are formed as a result of $\langle a \rangle$ and $\langle c + a \rangle$ dislocation interactions [43]. Figure 3(c) depicts the morphological effects related to surface step formation due to twinning on the examined ROI, which shows a tangent as high as 87.04°, with a height of 379.05 nm.

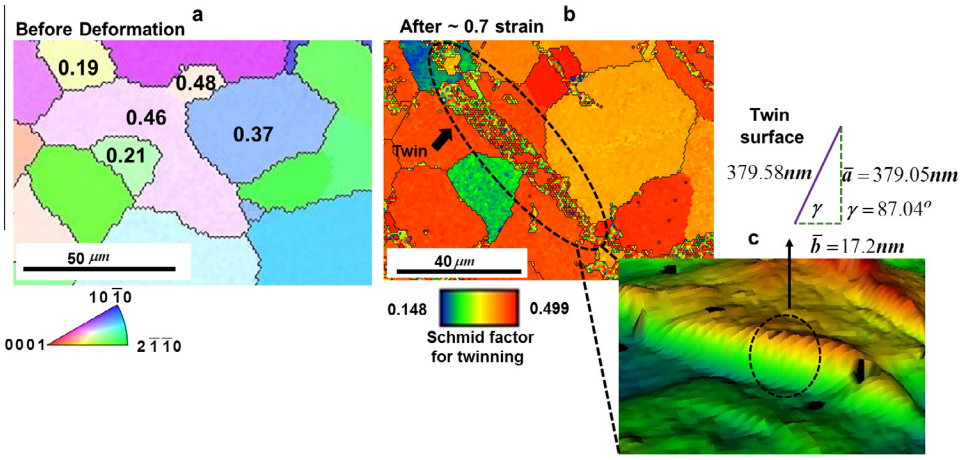

Figure 3. (a) KAM before deformation, (b) SF contour after deformation and (c) 3-D effects of twinning are evident on the surface and its corresponding edges in the ROI.

A closer inspection of the results in Figures 1–3 reveals significant strain and surface gradients within grains and near grain boundaries which can be conceivably reduced by secondary twins [17]. This letter further demonstrates the relationship between surface morphology evolution during compression of Mg alloys and twinning. Both in situ and ex situ grain-scale observations were used to demonstrate that twinning is responsible for large intrusions and extrusions that form inside and around twin-favorable grains. Direct evidence and quantification were provided to illustrate the 3-D nature of such twin-induced effects, which are very likely to be associated with both macroscale and microscale plasticity and fracture effects.

A.K. would like to acknowledge financial support from NSF CMMI Award No. 1434506. M.L.T. gratefully acknowledges funding from the Department of Energy through contract # NE0000315, and from the U.S. Nuclear Regulatory Commission through contract # NRC-38-10-928.

[1] I. Beyerlein, L. Capolungo, P. Marshall, R. McCabe, C. Tomé, Philos. Mag. 90 (2010) 2161–2190.
[2] A. Serra, D.J. Bacon, Philos. Mag. A 73 (1996) 333–343.
[3] J. Koike, Y. Sato, D. Ando, Mater. Trans. 49 (2008) 2792.
[4] H. El Kadiri, J. Baird, J. Kapil, A. Oppedal, M. Cherkaoui, S.C. Vogel, Int. J. Plast 44 (2013) 111–120.
[5] L. Leclercq, L. Capolungo, D. Rodney, Mater. Res. Lett. 2 (3) (2014) 1–8.
[6] N. Thompson, D.J. Millard, Philos. Mag. Ser. 7 (43) (1952) 422–440.
[7] Y. Yang, L. Wang, T.R. Bieler, P. Eisenlohr, M.A. Crimp, Metall Mat. Trans. A 42 (2011) 636–644.
[8] C.D. Barrett, H. El Kadiri, Acta Mater. 63 (2014) 1–15.
[9] I. Beyerlein, C. Tomé, Phys. Eng. Sci. 466 (2010) 2517–2544.
[10] J. Wang, I. Beyerlein, C. Tomé, Int. J. Plast 56 (2014) 156–172.
[11] I. Beyerlein, J. Wang, M. Barnett, C. Tomé, Phys. Eng. Sci. 468 (2012) 1496–1520.
[12] M. Yoo, Metall. Trans. A 12 (1981) 409–418.
[13] M. Barnett, Mater. Sci. Eng., A 464 (2007) 1–7.
[14] U. Kocks, D. Westlake, AIME Met. Soc. Trans. 239 (1967) 1107–1109.
[15] J. Hutchinson, Metall. Trans. A 8 (1977) 1465–1469.
[16] T. Bieler, P. Eisenlohr, F. Roters, D. Kumar, D. Mason, M. Crimp, D. Raabe, Int. J. Plast 25 (2009) 1655–1683.
[17] D. Ando, J. Koike, Y. Sutou, Acta Mater. 58 (2010) 4316–4324.
[18] D. Hull, Acta Metall. 8 (1960) 11–18.
[19] F. Yang, S. Yin, S. Li, Z. Zhang, Mater. Sci. Eng., A 491 (2008) 131–136.
[20] S. Suresh, Fatigue of Materials, Cambridge University Press, Cambridge, 1998.
[21] R. Zeng, E. Han, W. Ke, W. Dietzel, K.U. Kainer, A. Atrens, Int. J. Fatigue 32 (2010) 411–419.
[22] O. Muránsky, M. Barnett, D. Carr, S. Vogel, E. Oliver, Acta Mater. 58 (2010) 1503–1517.
[23] M.R. Barnett, M.D. Nave, A. Ghaderi, Acta Mater. 60 (2012) 1433–1443.
[24] K. Hazeli, J. Cuadra, P.A. Vanniamparambil, A. Kontsos, Scr. Mater. 68 (2013) 83–86.
[25] K. Hazeli, H. Askari, J. Cuadra, F. Streller, R.W. Carpick, H.M. Zbib, A. Kontsos, Int. J. Plast. 68 (2015) 55–76.
[26] S. Vaidya, S. Mahajan, Acta Metall. 28 (1980) 1123–1131.
[27] D. Raabe, M. Sachtleber, Z. Zhao, F. Roters, S. Zaefferer, Acta Mater. 49 (2001) 3433–3441.
[28] D. Raabe, M. Sachtleber, H. Weiland, G. Scheele, Z. Zhao, Acta Mater. 51 (2003) 1539–1560.
[29] Z. Zhao, M. Ramesh, D. Raabe, A. Cuitino, R. Radovitzky, Int. J. Plast 24 (2008) 2278–2297.
[30] S. Dave, X. Song, F. Hofmann, K. Dragnevski, A. Korsunsky, Procedia Eng. 1 (2009) 197–200.
[31] A. Tatschl, O. Kolednik, Mater. Sci. Eng., A 339 (2003) 265–280.
[32] J.D. Carroll, W. Abuzaid, J. Lambros, H. Sehitoglu, Int. J. Fatigue 57 (2013) 140–150.
[33] M.A. Sutton, J.-J. Orteu, H.W. Schreier, Image Correlation for Shape, Motion and Deformation Measurements: Basic Concepts, Theory and Applications, Springer, Berlin, 2009.
[34] K. Hazeli, A. Sadeghi, M.O. Pekguleryuz, A. Kontsos, Mater. Sci. Eng., A 578 (2013) 383–393.
[35] Y. Takayama, J.A. Szpunar, Mater. Trans. 45 (2004) 2316–2325.
[36] S.H. Park, S.-G. Hong, J.H. Lee, C.S. Lee, Mater. Sci. Eng., A 532 (2012) 401–406.
[37] X. Lou, M. Li, R. Boger, S. Agnew, R. Wagoner, Int. J. Plast 23 (2007) 44–86.
[38] S. Kleiner, P. Uggowitzer, Mater. Sci. Eng., A 379 (2004) 258–263.
[39] S. Yi, H.-G. Brokmeier, D. Letzig, J. Alloys Compd. 506 (2010) 364–371.
[40] K. Hazeli, A. Sadeghi, M. Pekguleryuz, A. Kontsos, Mater. Sci. Eng., A 589 (2013) 275–279.
[41] M. Meyers, O. Vöhringer, V. Lubarda, Acta Mater. 49 (2001) 4025–4039.
[42] L. Balogh, S. Niezgoda, A. Kanjarla, D. Brown, B. Clausen, W. Liu, C. Tomé, Acta Mater. (2013).
[43] D. Yin, K. Zhang, G. Wang, W. Han, Mater. Sci. Eng., A 392 (2005) 320–325.